Powder Technology 228 (2012) 424–428

Contents lists available at SciVerse ScienceDirect

Powder Technology

journal homepage: www.elsevier.com/locate/powtec

Short Communication

Deformed liquid marbles: Freezing drop oscillations with powders

J.O. Marston [a,*], Y. Zhu [a], I.U. Vakarelski [a,b], S.T. Thoroddsen [a,b]

[a] Division of Physical Sciences and Engineering, King Abdullah University of Science and Technology, Thuwal, 23955-6900, Saudi Arabia
[b] Clean Combustion Research Centre, King Abdullah University of Science and Technology, Thuwal, 23955-6900, Saudi Arabia

ARTICLE INFO

Article history:
Received 25 April 2012
Received in revised form 28 May 2012
Accepted 2 June 2012
Available online 9 June 2012

Keywords:
Drop impact
Rebound
Liquid marble
Splashing

ABSTRACT

In this work we show that when a liquid drop impacts onto a fine-grained hydrophobic powder, the final form of the drop can be very different from the spherical form with which it impacts. In all cases, the drop rebounds due to the hydrophobic nature of the powder. However, we find that above a critical impact speed, the drop undergoes a permanent deformation to a highly non-spherical shape with a near-complete coverage of powder, which then freezes the drop oscillations during rebound.

1. Introduction

The impact of liquid drops onto porous surfaces is an extremely important physical process, commonplace in many applications ranging from inkjet printers to granulation. When the target surface for the drop is a powder, the impact represents the first stage of the wetting and nucleation step [1] in the overall granulation process. Thus the topic has received renewed interest [2–6] in order to study phenomena such as the temporal evolution of the spreading phase, the maximum deformation of the drop and the resulting crater morphology.

The work of Hapgood and co-workers [7] has shown the possibility of using hydrophobic powder in the production of novel, hollow granules. When a liquid drop is completely covered by a hydrophobic powder, the resulting formation is referred to as a "liquid marble" [8], which are generally spherical in shape [9–16] when the initial drop diameter, D_0, is smaller than the capillary length. That is, when $D_0 \lesssim \sqrt{\sigma/\rho g}$, where g is the acceleration due to gravity and σ and ρ are the liquid surface tension and density respectively. The marble formation may buckle, however, during the drying stage [7] depending on the liquid viscosity and drying rate. Stable, non-spherical "armored" shells have previously only been observed for bubbles [17].

In this communication, we observe a novel feature of the impact dynamics of a water drop with a superhydrophobic powder. In particular, we find a critical impact speed beyond which the resulting marble is no longer spherical, but takes on a deformed cylindrical shape. The onset of the deformed shape occurs during the retraction of the drop, after it has reached the maximum spread on the powder surface. As such, we observe that the oscillations of the drop during rebound can be frozen.

2. Materials and methods

The experimental setup (see Fig. 1(a)) consists of a small cylindrical container, filled with fine glass beads. The beads have a mean diameter $d_{4,3} = 31\ \mu m$ ($d_{10} = 19\ \mu m$, $d_{90} = 46\ \mu m$) and circularity $C = \frac{4\pi A}{P^2} = 0.96$, as determined by particle size and shape analysis on a combination of a Malvern Mastersizer and Malvern Morphologi G3. The beads were hydrophobized using a commercial agent (Glaco Mirror Coat "Zero", Soft 99 Co.), which is an alcohol-based suspension of silica nanoparticles. The dry beads are first washed with ethanol by placing in an ultra-sonic cleaner for 15 min. The beads are then drained and over-saturated with the hydrophobizing agent before sonicating again for a further 15 min. Finally, the wet beads are drained and placed in a dessicator, which is evacuated to allow for complete evaporation of the solvent before heat-curing in a temperature-controlled furnace at 120 °C for 2 h. The beads are thus left with a stable coating of nano-scale structures formed by the silica particles. Fig. 1(b) shows an example SEM image of the nano-structures formed when this coating is deposited on a flat silicon wafer. A millimetric water drop placed on a glass microscope slide coated with this agent typically exhibits a contact angle of about 160 − 170°.

In the impact experiments, we use pure water as the liquid and release a drop with diameter $D_0 = 2.1$ mm from heights $h_r \approx 1$ mm up to 40 cm. The drops thus impact vertically with speed $V_0 = \sqrt{2gh_r} = 0.14$–$2.8$ m/s, which is measured directly from the video sequences. The main dimensionless parameter for the impact is the Weber number, $We = \rho D_0 V_0^2/\sigma$, which varies from ~0.5 to 230. The Bond number for this study, $Bo = \rho g D_0^2/\sigma = 0.59$ and the

* Corresponding author.
E-mail address: jeremy.marston@kaust.edu.sa (J.O. Marston).

0032-5910/$ – see front matter © 2012 Elsevier B.V. All rights reserved.
doi:10.1016/j.powtec.2012.06.003

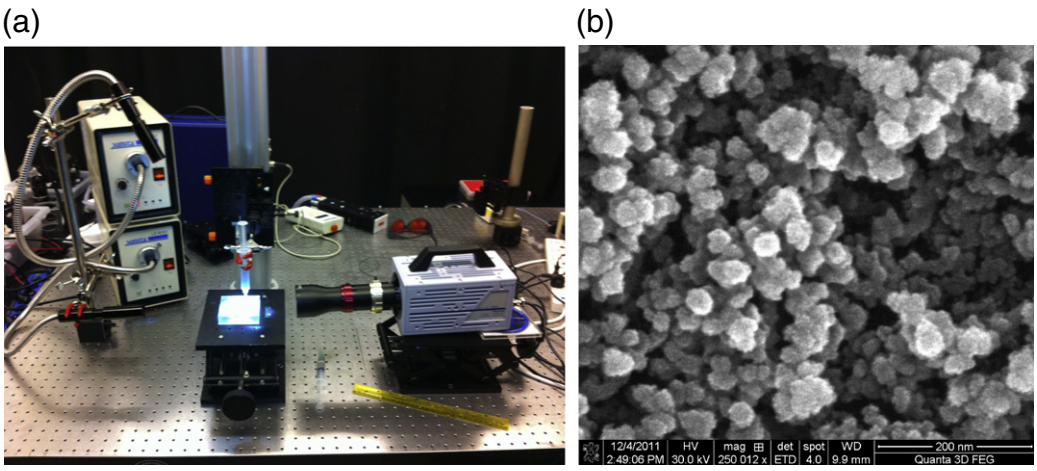

Fig. 1. (a) Photograph of the experimental setup. (b) SEM image of the Glaco mirror coat "Zero" deposited on a plain silicon wafer.

Ohnesorge number, $Oh = \mu/\sqrt{\rho\sigma D_0} = 2.6 \times 10^{-3}$. The impact and subsequent rebound dynamics are captured by a high-speed video camera (Photron Fastcam SA-3 or SA-5) equipped with a 1× objective lens, which yields effective pixel sizes of 17 and 20 μm/px respectively. Frames rates up to 10,000 fps were used.

3. Results

Fig. 2 shows sequences from high-speed video clips of the impact and rebound of water drops from the hydrophobic powder surface. The impact speeds in these sequences are $V_0 = 0.98$, 1.25, 1.64 and

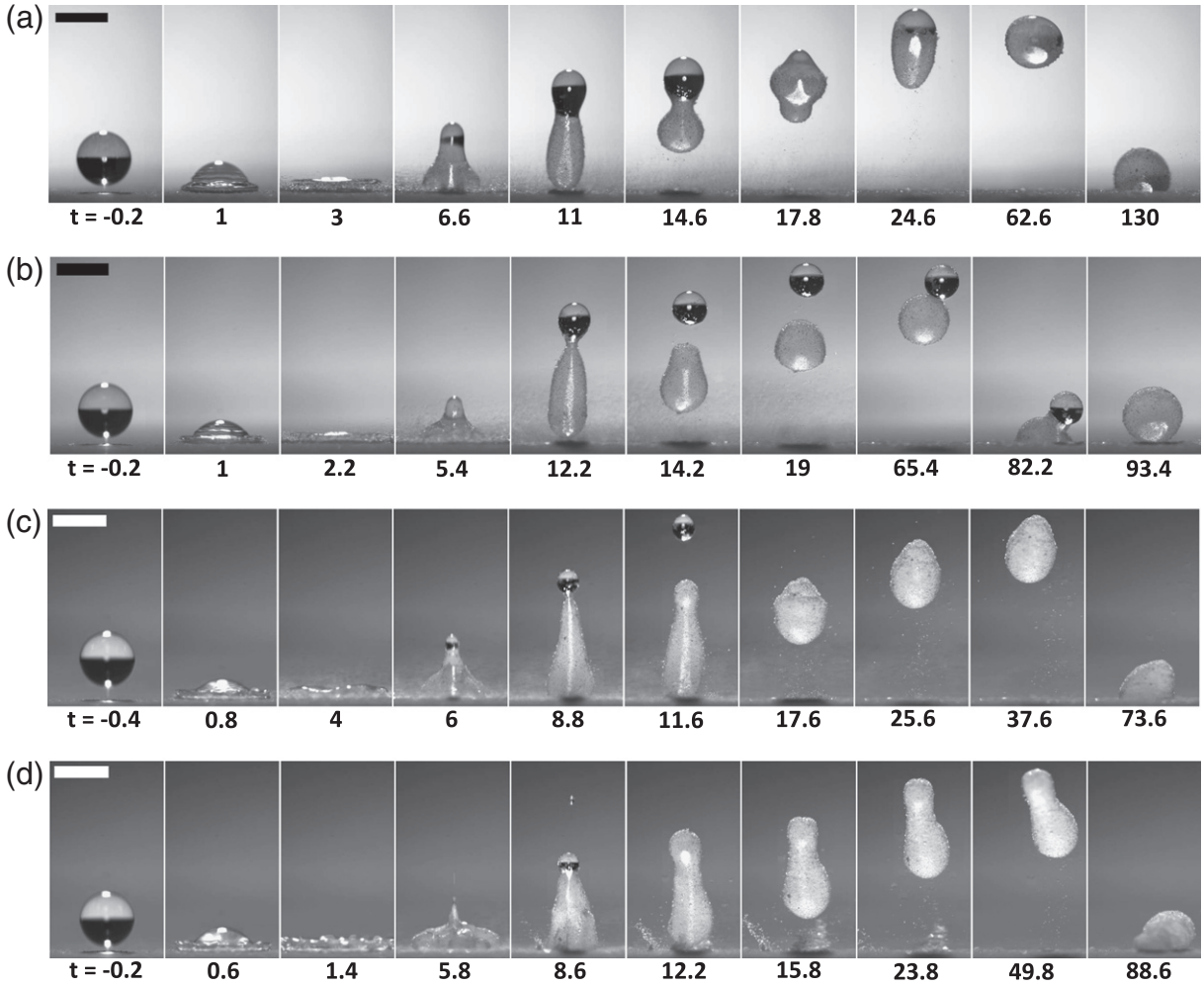

Fig. 2. Sequences taken from high-speed video clips for the impact and rebound of water drops ($D_0 = 2.1$ mm) onto hydrophobic powder. Impact speeds: (a) $V_0 = 0.98$ m/s, (b) $V_0 = 1.25$ m/s, (c) $V_0 = 1.64$ m/s, (d) $V_0 = 1.84$ m/s. Times (in milliseconds) from initial contact are given below each panel. The scale bars each represent 2 mm. See also the supplemental movie for these sequences.

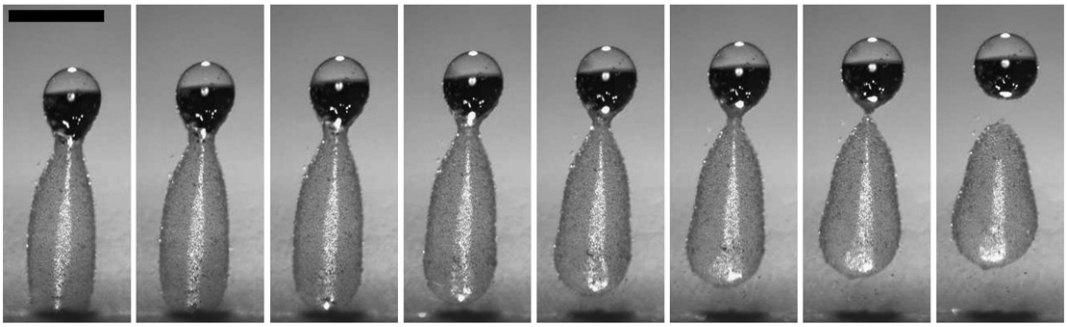

Fig. 3. Pinch-off of the satellite drop for $V_0 = 1.25$ m/s. First frame shown occurs at $t = 11$ ms after initial contact and subsequent frames are separated by 0.4 ms.

1.84 m/s respectively. The first four frames in each sequence are qualitatively similar, showing the initial spreading-retraction stage. However, upon rebound we observe vastly different dynamics. In Fig. 2(a) for $V_0 = 0.98$ m/s, the drop remains as a single volume of fluid, with no satellite drop detachment and a partial coverage of powder. In Fig. 2(b) for $V_0 = 1.25$ m/s, a satellite drop is generated from the top of the drop, and the pinch-off occurs roughly at the extent of the powder coating (see close-up sequence in Fig. 3). This satellite drop then rejoins the main drop, but does not coalesce until the main drop re-impacts the powder surface. After coalescence, a liquid marble is formed. Once above a critical speed, $V_0^* \approx 1.6$ m/s, the satellite drop is fully ejected at higher speed and the main drop does not regain its spherical shape, as shown in Fig. 2(c) for $V_0 = 1.64$ m/s, where it has a slightly oblate appearance. For higher impact speeds, the deformation of the main drop becomes even more pronounced, as shown by Fig. 2(d) for $V_0 = 1.84$ m/s. The deformed marbles in Fig. 2(c) and (d) reach their new equilibrium shapes approximately 25 ms after first contact and do not change shape again until they re-impact the powder surface. See also the supplemental videos.

Fig. 3 shows a close-up sequence of the pinch-off of the top satellite drop. Here, we can readily observe that the separation occurs approximately at the extent of the powder coating, so that the satellite is relatively "clean" with few grains on the surface, whilst the main drop has a complete powder coverage. When a top satellite drop is generated, we find that the pinch-off always occurs in this fashion, i.e. a fully covered main drop and a relatively clean satellite drop. A similar observation was made for the rebound of glycerol drops pinned to the powder surface [2]. It thus appears that the amount of powder absorbed into the drop surface, along with the occurrence of the pinch-off, is instrumental in the deformation of the marbles since the pinch-off then results in the remainder of the drop being completely covered in the powder, after which the surface area becomes fixed, thus prohibiting further oscillatory motion.

Fig. 4 shows snapshots of the deformed marble shapes for different impact speeds. These snapshots were taken close to the full rebound height, after which the shape does not change until the marble re-impacts the powder bed. The liquid volume of each marble depends on the impact speed, since the satellite drop volume generally decreases as the impact speed increases. A priori, these deformed shapes may have been presumed to result from the coalescence (or partial coalescence) of multiple liquid marbles, rather than the freezing of the drop oscillations.

Fig. 5(a) plots the maximum spread diameter against the impact speed, showing a linear increase with speed until a critical value of approximately 2.2 m/s, after which prompt splashing occurs with the ejecta lifted off the surface. This causes the sharp drop in D_{max} shown in Fig. 5(a) for $V_0 = 2.61$ m/s. The different symbols used here depict the different phenomena observed and, in particular, the filled symbols show the parameter range where we observe the "deformed" marble formations, such as those shown in Fig. 2(c) and (d) and Fig. 4(a–d).

Previously, Marston et al. [2] found that the maximum spread of low-viscosity liquid drops on (untreated) powders scales as $D_{max}/D_0 \sim We^{1/5}$, which was later confirmed by [6]. Here, however, we find a much stronger dependence on the impact Weber number whereby the maximum spread scales approximately as $We^{2/5}$, as shown by the log-log plot in Fig. 5(b). This then indicates that $D_{max} \sim V_0^{4/5}$ for drops spreading on hydrophobic powders. The same 2/5 dependence on the Weber number was also found for drops impacting superheated surfaces [18], however, the relation between the two experiments is far from clear.

Finally, to quantify the deformation of the liquid marbles, we perform two calculations on the two-dimensional profiles in the video sequences–namely–the circularity, C and the deviation from the equivalent circular radius, S. First, we determine the area, A and perimeter, P from a binarized version of the raw image. The circularity

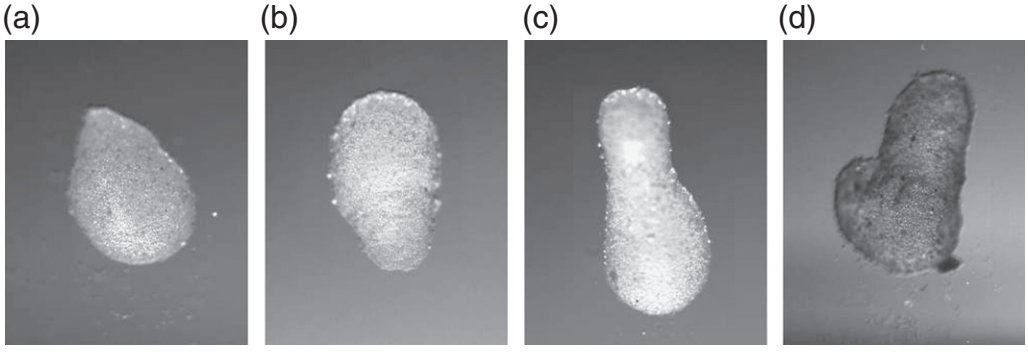

Fig. 4. Images of the deformed marble shape, near full rebound height, which is frozen until the marble re-impacts the powder surface. Impact speeds are $V_0 = 1.61$, 1.66, 1.84, 1.97 m/s respectively.

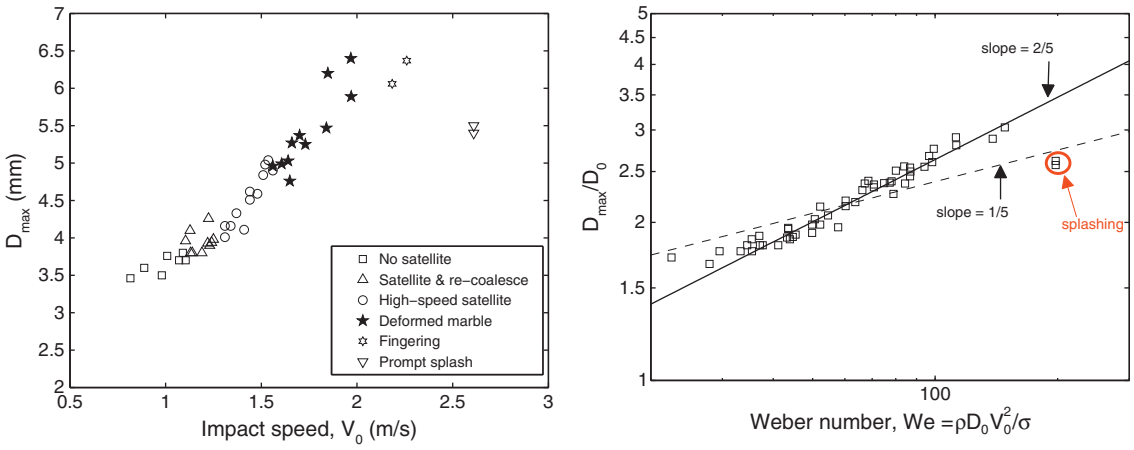

Fig. 5. (a) Maximum deformation diameter, D_{max}, versus impact speed, V_0. The different symbols correspond to different general phenomenon observed. (b) Normalised maximum spread, D_{max}/D_0, versus impact Weber number $We=\rho D_0 V_0^2/\sigma$ with slopes of 1/5 (dashed line) and 2/5 (solid line).

is then given simply by $C=4\pi A/P^2$. For the deviation, we must first calculate the equivalent circular radius, $r_{circ}=\sqrt{A/\pi}$. The perimeter, P is then extracted in matrix form and the distance from the centroid to each discrete point (i.e. each pixel) on the perimeter is calculated as r_i. Images of the marbles near the full rebound height are shown in Fig. 6, where the perimeters and centroids (as determined by image processing) have been highlighted. We then calculate the deviation from the equivalent circular radius as

$$S=\sqrt{\frac{1}{n}\sum_{i=1}^{n}(r_i-r_{circ})^2}.$$

The circularity and deviation measurements are plotted versus the impact speed in Figs. 7(a) and (b) respectively. In Fig. 7(a), we observe two distinct regimes–one for impact speeds below the critical speed, V_0^*, and one for speeds a little above the critical value. Note that there is a small transition region around the value $V_0=1.56-1.6$ m/s. For $V_0<V_0^*$, we find the marble formations are reasonably spherical with $C\approx 0.9$, where this value is lower than expected due to some small clusters of grains on the surface of the drop yielding a rougher perimeter. For $V_0>V_0^*$, the marble formations become clearly non-spherical with $C\approx 0.65-0.7$.

The deviation, S, plotted in Fig. 7(b) provides us with a much clearer distinction between the two regimes. Here, the transition for impact speeds around the critical value is much sharper with $S\approx 1$ for $V_0<V_0^*$, which then rises rapidly to $S\approx 19-20$ for $V_0>V_0^*$ for the deformed marbles. Clearly, the two-dimensional projection from the video sequence does not fully reflect the three-dimensional shape for the most deformed marbles (e.g. Fig. 4(d)). Rather, the calculations in Fig. 7(b) provide lower bounds for the deviation from a fully spherical shape.

4. Concluding remarks

We have performed an experimental study of the impact of water drops onto a bed of spherical, hydrophobic glass beads. In all cases, for drop release heights $h_r\gtrsim 2$ mm, the drop rebounded off the powder surface, however, we observed several distinct regimes, depending on the impact speed as follows:

1. $V_0<1.1$ m/s: The rebounding drop will remain whole with a partial powder coating.
2. $V_0\geq 1.14$ m/s: A satellite drop is ejected from the top of the drop.
3. $V_0<1.4$ m/s: The satellite will coalesce with the main drop and the pinch-off generally occurs at the extent of the powder coating, which adheres to the drop during the spreading phase of the impact.
4. $V_0\geq 1.56$ m/s: The main drop does not regain its spherical shape and we observe a deformed liquid marble, which freezes the oscillatory motion during rebound.
5. $V_0\geq 2.27$ m/s: Prompt splashing occurs, where the main drop becomes a deformed marble and several spherical satellite marbles are also formed.

In contrast to previous observations, we find that the normalised maximum drop diameter scales as $D_{max}/D_0\sim We^{2/5}$. Given the highly non-spherical shapes observed of the marbles observed in this work, the granule morphology studied by Emady et al. [3] needs to be extended to investigate powders with variable wettability. To

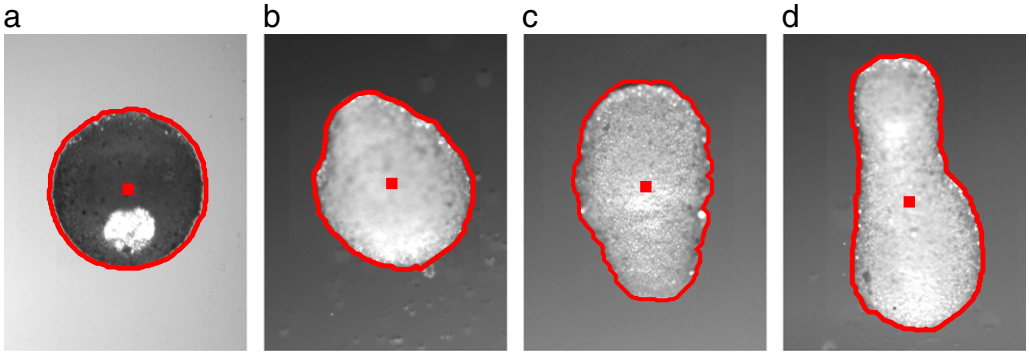

Fig. 6. Marble formations with highlighted boundaries and centroids determined by image processing for (a) $V_0=1.14$ m/s, (b) $V_0=1.56$ m/s, (c) $V_0=1.66$ m/s, and (d) $V_0=1.84$ m/s.

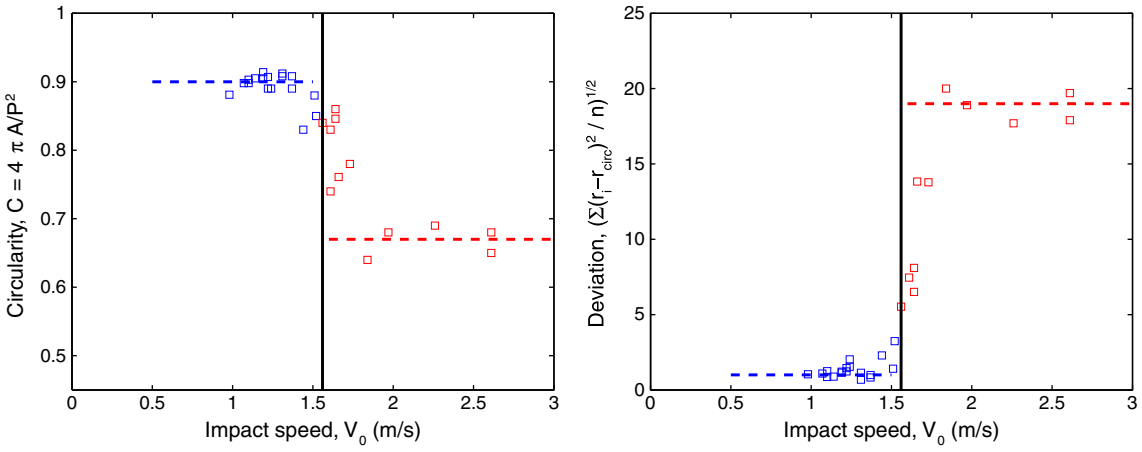

Fig. 7. (a) Circularity, $C = 4\pi A/P^2$ and (b) Deviation from circular profile (see text for definition) both versus impact speed, V_0. In both, the black line indicates the critical speed $V_0 = 1.56$ m/s. Blue data points are below this threshold, while red data points are above it. The dashed blue and red lines are approximate constant fits to the data in the spherical and deformed marble regimes.

our knowledge, the observations herein constitute the first report of deformed marbles produced by the impact of water drops and are part of an ongoing investigation into the dynamic interaction of liquid drops with hydrophobic powders.

Supplementary data to this article can be found online at http://dx.doi.org/10.1016/j.powtec.2012.06.003.

Acknowledgement

This work was partially supported by an Academic Excellence Alliance grant (7000000028) awarded by the KAUST Office of Competitive Research Funds.

References

[1] S.M. Iveson, J.D. Lister, K. Hapgood, B.J. Ennis, Nucleation, growth and breakage phenomena in agitated wet granulation processes: a review, Powder Technology 117 (2001) 3–39.
[2] J.O. Marston, S.T. Thoroddsen, W.K. Ng, R.B.H. Tan, Experimental study of liquid drop impact onto a powder surface, Powder Technology 203 (2010) 223–236.
[3] H.N. Emady, D. Kayrak-Talay, W. Schwerin, J.D. Lister, Granule formation mechanisms and morphology from single drop impact on powder beds, Powder Technology 212 (2011) 69–79.
[4] H. Katsuragi, Morphology scaling of drop impact onto a granular layer, Physical Review Letters 104 (2011) 218001.
[5] H. Katsuragi, Length and time scales of a liquid drop impact and penetration into a granular layer, Journal of Fluid Mechanics 675 (2011) 552–573.
[6] E. Nefzaoui, O.R. Skurtys, Impact of a liquid drop on a granular-medium: inertia, viscosity and surface tension effects on the drop deformation, Experimental Thermal and Fluid Science (2012), http://dx.doi.org/10.1016/j.expthermflusci.2012.03.007.
[7] N. Eshtiaghi, J.S. Liu, K.P. Hapgood, Formation of hollow granules from liquid marbles: small scale experiments, Powder Technology 197 (2010) 184–195.
[8] G. McHale, M.I. Newton, Liquid marbles: principles and applications, Soft Matter 7 (2011) 5473–5481.
[9] P. Aussillous, D. Quere, Properties of liquid marbles, Proceedings of the Royal Society A 462 (2006) 973–999.
[10] L. Gao, J. McCarthy, Ionic liquid marbles, Langmuir 23 (2007) 10445–10447.
[11] K.P. Hapgood, B. Khanmohammadi, Granulation of hydrophobic powder, Powder Technology 189 (2009) 253–262.
[12] N. Eshtiaghi, J.S. Liu, W. Shen, K.P. Hapgood, Liquid marble formation: spreading coefficients or kinetic energy? Powder Technology 196 (2009) 126–132.
[13] Y. Xue, H. Wang, Y. Zhao, L. Dai, L. Feng, X. Wang, T. Lin, Magnetic liquid marbles: a “precise” miniature reactor, Advanced Materials XX (2010) 1–6.
[14] Y. Zhao, J. Fang, H. Wang, X. Wang, T. Lin, Magnetic liquid marbles: manipulation of liquid droplets using highly hydrophobic Fe−3O−4 nanoparticles, Advanced Materials 22 (2010) 707–710.
[15] E. Bormashenko, R. Pogreb, A. Musin, R. Balter, G. Whyman, D. Aurbach, Interfacial and conductive properties of liquid marbles coated with carbon black, Powder Technology 203 (2010) 529–533.
[16] N. Estiaghi, K.P. Hapgood, A quantitative framework for the formation of liquid marbles and hollow granules from hydrophobic powders, Powder Technology 223 (2012) 65–76.
[17] A.B. Subramaniam, M. Abkarian, L. Mahadevan, H. Stone, Non-spherical bubbles, Nature 438 (2005) 930.
[18] T. Tran, H.J.J. Staat, A. Prosperetti, C. Sun, D. Lohse, Physical Review Letters 108 (2012) 036101.